Equivalency of geologic and geodetic rates in contractional orogens: New insights from the Pamir Frontal Thrust

Tao Li,[1] Jie Chen,[1] Jessica A. Thompson,[2] Douglas W. Burbank,[2] and Weipeng Xiao[1,3]

Received 24 May 2012; revised 23 June 2012; accepted 25 June 2012; published 7 August 2012.

[1] Across contractional orogens, the equivalency between decadal convergence rates from geodetic GPS data and geologic shortening rates at time scales of thousands or millions of years has rarely been documented. Here, we present an example from the northern margin of Chinese Pamir, where the Main Pamir Thrust is tectonically quiescent, and recent deformation is concentrated on the Pamir Frontal Thrust (PFT). Based on dated and faulted fluvial terraces, magnetostratigraphy, and mapping, the horizontal shortening rate of the PFT is ~6–7 mm/a at time scales of both ~18.4 ka and ~0.35 Ma, comparable to the geodetic rate of ~6–9 mm/a across the same zone, implying that modern geodetic rates are a reasonable proxy for geologic rates since ~0.35 Ma. Comparing this example with studies in other contractional orogens, we conjecture that a match or mismatch of geologic-geodetic rates typically depends on the time scale of observation, fault geometry, and fault mechanics. **Citation:** Li, T., J. Chen, J. A. Thompson, D. W. Burbank, and W. Xiao (2012), Equivalency of geologic and geodetic rates in contractional orogens: New insights from the Pamir Frontal Thrust, *Geophys. Res. Lett.*, *39*, L15305, doi:10.1029/2012GL051782.

1. Introduction

[2] The proliferation of GPS data on relative velocities across orogens and plate boundaries has provided a far more complete view of the modern patterns of crustal deformation. Although it is tempting to use these decadal rates as proxies for rates applicable to thousands or millions of years, this equivalency has rarely been tested in contractional orogens. Along some well-studied strike-slip faults, such as the southern San Andreas fault where numerous paleoseismic studies define slip rates at time scales of hundreds of years, geologic and geodetic rates appear quite closely matched [*Segall*, 2002]. Across contractional orogens, however, mismatches are more common than matches. For example, in the Himalaya, geomorphic studies at Holocene time scales clearly show that ~20 mm/a of slip occurs along the Main Frontal Thrust [*Lavé and Avouac*, 2000], whereas geodetic shortening across the same zone is only a few millimeters per year [*Cattin and Avouac*, 2000; *Avouac*, 2003]. Similar mismatches are observed across the Taiwanese orogen [*Dominguez et al.*, 2003]. In contrast, across the Kyrgyz Tian Shan, cumulative late-Quaternary rates on major faults spanning the range provide a good match to the geodetic rates [*Thompson et al.*, 2002]. When these Kyrgyz geodetic rates are used to estimate the initiation age of mountain building [*Abdrakhmatov et al.*, 1996], however, they predict a much younger age than that deduced from thermochronology and magnetostratigraphy [*Yin et al.*, 1998; *Sobel et al.*, 2006], implying much slower geologic rates at longer time scales.

[3] Here we present shortening rates of the Pamir Frontal Thrust (PFT) along the northern margin of Chinese Pamir (Figure 1a). Our new data indicate that shortening rates of the PFT adjacent to the Mayikake basin (~75 km west of Kashgar) are similar at time scales of both ~0.35 Ma and ~18.4 ka and comparable to the decadal geodetic rate across the same zone. Hence, the geodetic rate of the PFT appears to yield a reasonable proxy for the long-term geologic rate. Comparing this example with previous studies, we investigate the time scale for which the geodetic rates can be reliably extrapolated to represent geologic rates and define factors that may modulate the equivalence of geologic and geodetic rates.

2. Modern Convergence Rate Along the PFT From Geodetic GPS Data

2.1. Deformation Along the Northern Margin of Chinese Pamir

[4] The Pamir lies in the northwestern region of the Indo-Asian collision zone. During Cenozoic times, the northern margin of the Pamir has indented northward ~300 km, as it was accommodated by south-dipping intracontinental subduction along the Main Pamir Thrust (MPT) and was coupled to strike-slip faulting on its western and eastern margins [*Burtman and Molnar*, 1993] (Figure 1a). In westernmost China, geologic deformation is concentrated on the MPT along the Pamir's oblique eastern margin, on the PFT along the leading edge of deformation, and on the piggyback basin between them (Figure 1c).

[5] The MPT, separating domains with contrasting geology and geomorphology, comprises several high-angle reverse faults involving pre-Cenozoic basement [*Chen et al.*, 2010], with slip initiating sometime between 25–20 Ma [*Sobel and Dumitru*, 1997]. Geologic mapping and rare earthquakes (Figure 1c), however, indicate low Holocene activity along the thrust.

[6] The 30- to 40-km-wide piggyback basin north of the MPT exhibits little geomorphic expression of active structures (Figure 1c). In the subsurface, however, three seismically imaged imbricate thrusts are interpreted to represent the northward propagation of the MPT (Figure 1d) [*Chen et al.*,

[1]State Key Laboratory of Earthquake Dynamics, Institute of Geology, China Earthquake Administration, Beijing, China.
[2]Departhment of Earth Science, University of California, Santa Barbara, California, USA.
[3]Anhui Earthquake Administration, Hefei, China.

Corresponding author: J. Chen, State Key Laboratory of Earthquake Dynamics, Institute of Geology, China Earthquake Administration, Beijing 100029, China. (chenjie@ies.ac.cn)

0094-8276/12/2012GL051782

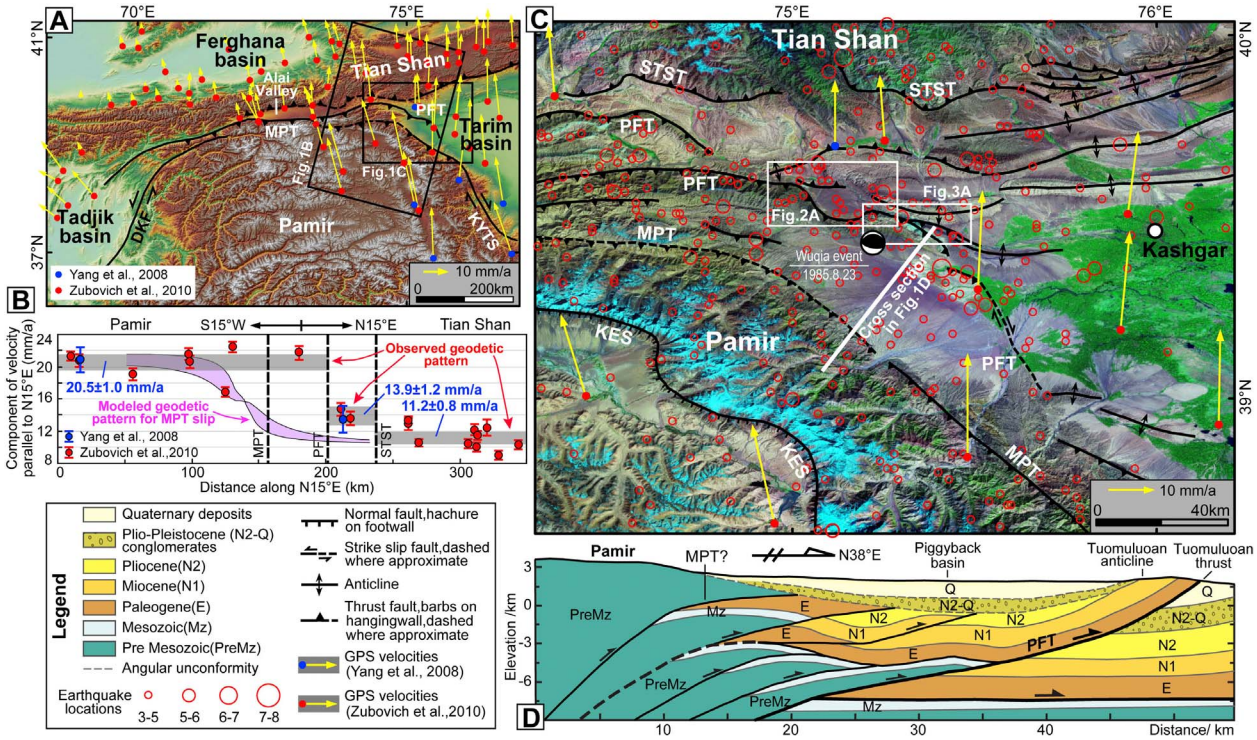

Figure 1. (a) Topography of the Pamir and surrounding area with local GPS vectors. Box encloses GPS sites used in Figure 1b. (b) N15°E component of GPS velocities (perpendicular to the PFT trend) across the Main Pamir Thrust (MPT), Pamir Frontal Thrust (PFT) and South Tian Shan Thrust (STST), showing ~6–9 mm/a of convergence across the PFT. The gray bar represents mean value and standard error of velocities. Purple field shows predicted geodetic pattern for MPT slip from an elastic half-space model with a creeping detachment depth of 6–17 km (see auxiliary material). Locations of the MPT, PFT and STST are not exact due to map projection. (c) GPS vectors projected on an ASTER image of the field area. See Figure 1a for location. Earthquake locations from the USGS seismic catalog for the period 1973–2010. (d) Interpreted seismic line KS99-610 between the MPT and PFT from *Chen et al.* [2010]. Location in Figure 1c. DKF-Darvaz-Karakul Fault, KES-Kongur Extension System, KYTS-Kashgar-Yecheng Transfer System. GPS velocities relative to Eurasia from *Yang et al.* [2008] and *Zubovich et al.* [2010].

2010]. These faults are overlain by largely undeformed piggyback-basin Plio-Quaternary deposits, indicating that slip on these thrusts has apparently ceased and deformation has been transferred to the PFT along a detachment surface localized within Paleogene gypsum.

[7] The PFT is a zone of active thrust faulting and folding that can be subdivided into several segments based on different deformation characteristics (Figure 1c). For example, in the Mayikake basin, the PFT includes the Biertuokuoyi Frontal Thrust and the Mayikake Thrust (Figure 2a), whereas further east, it includes the Tuomuluoan Thrust and thrust-related Tuomuluoan anticline (Figure 3a). Widely distributed active structures and frequent earthquakes, including the 1985 Wuqia M7.4 event (Figure 1c) [*Feng*, 1994], reflect ongoing activity on the PFT and contrast with the quiescent MPT to its south.

2.2. Modern Convergent Rate Along the PFT

[8] A swath of 22 GPS sites that is oriented N15°E (perpendicular to the PFT, Figure 1a) and spans the MPT, PFT and Southern Tian Shan Thrust (STST) serves to constrain the modern convergence rate of the PFT. GPS velocities in the Pamir and those bracketing the MPT are similar, with an average of 20.5 ± 1.0 mm/a relative to stable Eurasia (Figure 1b). Across the PFT, velocities abruptly drop to

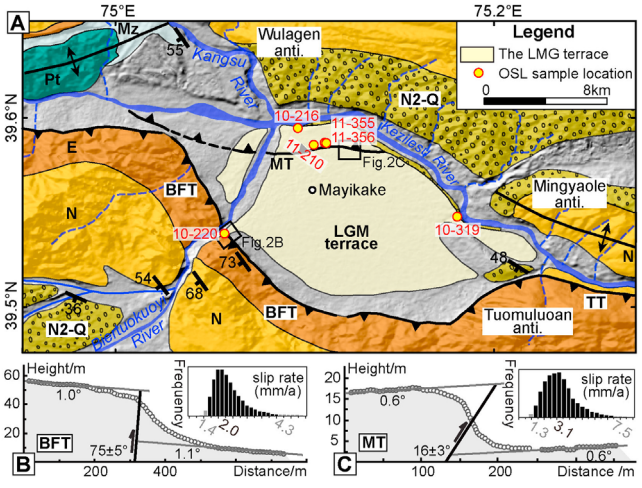

Figure 2. (a) Simplified geologic map of the Mayikake basin (location in Figure 1c): BFT-Biertuokuoyi Frontal Thrust, MT-Mayikake Thrust, and TT-Tuomuluoan Thrust. The prefix "LED" of OSL sample number is omitted. Same legend as Figure 1. (b and c) Topographic survey profiles across thrust scarps and Monte Carlo simulation results of the BFT and MT, respectively.

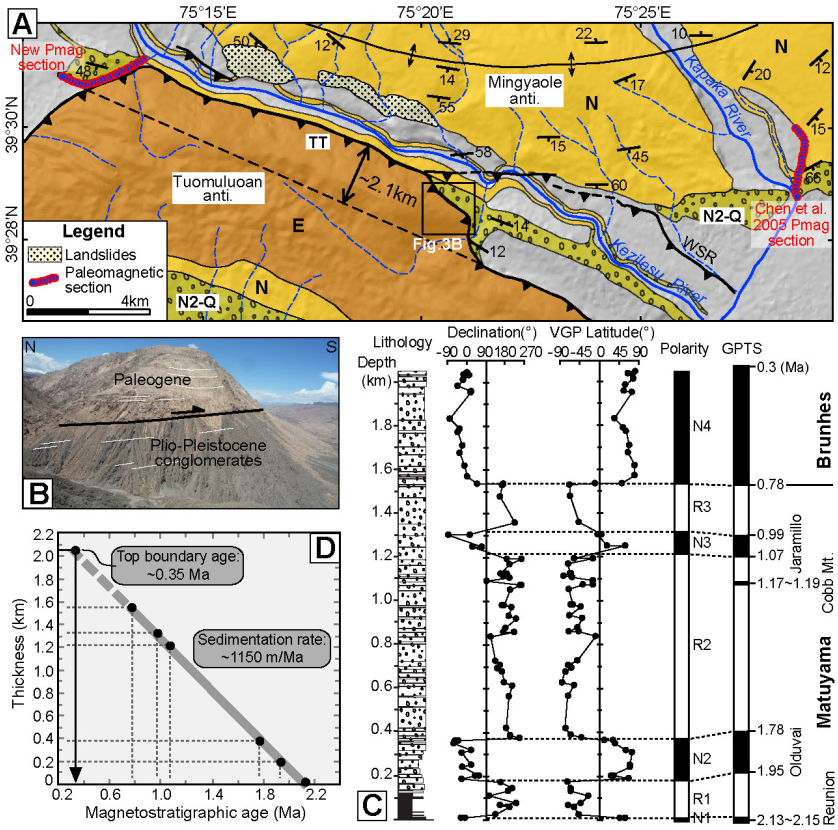

Figure 3. (a) Geologic map of the Tuomuluoan Thrust (TT) and surrounding area showing a minimum overthrusting width of ~2.1 km between Paleogene and Pleistocene strata. WSR-1985 Wuqia earthquake surface rupture. Location map in Figure 1c. Same legend as Figure 1. (b) Field photo of the TT outcrop, exposing Paleogene units overthrusting Pleistocene conglomerate. Outcrop location marked in Figure 3a. (c) Magnetostratigraphy of the Pleistocene conglomerate section as correlated with the time scale of *Lourens et al.* [2004]. (d) Thickness as a function of magnetostratigraphic age. Upward extrapolation of the nearly uniform sedimentation rate seen from ~2.15 to 0.8 Ma implies an age of ~0.35 Ma for the top of the section.

13.9 ± 1.2 mm/a, and across the STST to the north, velocities average ~11.2 ± 0.8 mm/a. Although both slip and elastic strain accumulation are difficult to isolate on individual faults due to sparse GPS sites, elastic half-space modeling suggests the geodetic data are incompatible with slip on a temporarily "locked" MPT (Figure 1b and auxiliary material) and supports slip cessation of the MPT.[1] Whereas the STST may also accumulate elastic strain, low Quaternary slip [*Scharer et al.*, 2006; *Heermance et al.*, 2008] and absence of evidence for significant earthquakes on the STST near the Mayikake basin indicate the geodetic rate accommodated by the STST is very limited, and the major convergence is concentrated on the PFT. Assuming that elastic strain accumulation on the PFT does not extend over the surface traces of the MPT and the STST, GPS velocities bracketing the PFT yield a minimum convergent rate of 6.6 ± 1.1 mm/a along the PFT. If elastic strain accumulation were assumed to extend beyond surface traces of the MPT and the STST, GPS velocities across this wider zone yield a maximum convergent rate of 9.3±0.9 mm/a. In either case, the modern convergent rate across the PFT is ~6–9 mm/a, irrespective of whether or not elastic strain accumulation on the PFT extends over surface traces of the MPT and the STST.

[9] The epicenter of the Wuqia M7.4 earthquake in 1985 occurred within the GPS swath (Figure 1c). This event could have introduced a component of postseismic relaxation that would influence the geodetic measurements. Such an effect, however, is likely small because the regional contraction is sufficiently large to overwhelm the decades-old, transient response, and it cannot be responsible for the far-field contraction that is clear in the GPS data.

3. Shortening in the Mayikake Basin Since ~18.4 Ka

3.1. The Mayikake Basin

[10] The Mayikake basin, named after Mayikake village (Figure 2a), is a 15-km-long by 10-km-wide, SE-trending basin. Bounded by the Kezilesu River and structures exposing Cenozoic bedrock, the basin results from collision between the irregular margins of the Pamir and the Tian Shan. Major active structures in the basin are the Biertuokuoyi Frontal Thrust along its southwestern margin and the Mayikake Thrust across its northern part.

[11] The Mayikake basin is dominated by a wide, planar, gently N-sloping terrace surface, underlain by bedrock

[1]Auxiliary materials are available in the HTML. doi:10.1029/2012GL051782.

Table 1. OSL Dating Results (2σ) for Samples Taken From the LGM Terrace in the Mayikake Basin[a]

Sample Number	Latitude/Longitude	Depth (m)	Lithology	Equivalent Dose (Gy)	Dose Rate (Gy/ka)	Age (ka)
LED10-216	39.5948°N/75.0907°E	3.4	Muddy silt	47.2 ± 9.8	2.6 ± 0.8	18.2 ± 5.0
LED10-220	39.5391°N/75.0587°E	5.4	Muddy silt	44.1 ± 8.2	2.5 ± 0.6	17.6 ± 4.0
LED10-319	39.5451°N/75.1844°E	3.9	Muddy silt	49.0 ± 10.6	2.5 ± 0.8	19.4 ± 5.7
LED11-210	39.5811°N/75.0957°E	1.9	Muddy silt	62.8 ± 2.8	2.3 ± 0.6	27.6 ± 2.6
LED11-355	39.5833°N/75.1043°E	2.7	Muddy silt	76.5 ± 13.8	2.1 ± 0.4	35.8 ± 6.7
LED11-356	39.5833°N/75.1043°E	3.1	Muddy silt	68.3 ± 7.2	2.3 ± 0.6	29.4 ± 3.9

[a]Sampling, 4–11 μm fine-grained quartz separation and measurements follow standard methods [*Liu et al.*, 2010; *Lu et al.*, 2007] (see auxiliary material). Measurements were made in the State Key Lab. of Earthquake Dynamics, Inst. of Geology, China Earthquake Admin.

comprising Plio-Pleistocene conglomerates along the Kezilesu River, as well as Paleogene mudstone and limestone along the Biertuokuoyi River (Figure 2a). In order to constrain the age of the main terrace surface spanning the Mayikake basin, six optically stimulated luminescence (OSL) samples were taken from silt lenses in terrace deposits (Figure 2a and Table 1). Three samples yielded older ages than the other three. Considering the OSL dating of fluvial deposits may produce older results due to poor bleaching, we average the three younger ages to 18.4 ± 4.8 ka (2σ) to represent the terrace age, implying that this terrace was abandoned near the end of the Last Glacial Maximum (LGM) stage [*Petit et al.*, 1999]. We, therefore, define this terrace as the "LGM" terrace.

3.2. The Biertuokuoyi Frontal Thrust (BFT)

[12] Where best exposed, a ~13-km-long lateral ramp of the Biertuokuoyi Frontal Thrust (BFT) (Figures 1c and 2a) displaces both the Biertuokuoyi River terraces and Holocene alluvial fans at mountain front to create a series of SW-side-up fault scarps (Figure 2b). In the hanging wall, terrace deposits overlie Paleogene, SW-dipping marine sedimentary rocks. Incised terraces along the Biertuokuoyi River reveal Paleogene units faulted over fluvial deposits along a 75 ± 5°SW-dipping fault plane. Extensive striae with a rake of ~34° on the fault plane (see auxiliary material) indicate an ~3:2 ratio of strike-slip to dip-slip motion.

[13] Local differential GPS surveys of the LGM terrace surface across the thrust scarp (Figure 2b) reveal a vertical separation of ~38 m. Based on separation, surface slopes, known thrust location, observed fault dip, and the age of 18.4 ± 4.8 ka described above, Monte Carlo simulations (see auxiliary material) [*Thompson et al.*, 2002] define a dip-slip rate of 2.0 + 2.3/−0.6 mm/a (2σ) across the BFT (Figure 2b). Given the striae rake of ~34°, the total slip rate is ~3.6 mm/a. Because the BFT is interpreted to dip only 12° at depth (Figure 1d), the shortening rate can be approximated by the total slip rate at the surface. The component of BFT shortening rate in the N15°E orientation of the GPS swath is ~2.9 mm/a.

3.3. The Mayikake Thrust (MT)

[14] As a W-trending and N-dipping fault, the scarp of the Mayikake Thrust (MT) extends at least ~12 km (Figure 2a), crosses both the LGM terrace surface and nested terraces of the Biertuokuoyi River, and is buried under young alluvial fans. The thrust includes 2–3 splays and small anticlines near the easternmost and westernmost termini. Topographic fault scarps face south, opposite to the slope of the LGM terrace surface. Incision of modern channels across the thrust scarps exposes the near-surface dip of the thrust at two sites as 15±2° and 18±3°.

[15] The surveyed profile of the faulted LGM terrace (Figure 2c) reveals a vertical separation of ~15 m. Based on parameters outlined above, Monte Carlo simulations yield a dip-slip rate of 3.1 + 4.1/−1.8 mm/a (2σ) for the MT. Although subsurface geometries of the MT are unknown, it is reasonable to use the horizontal component of the dip-slip rate ~3.0 mm/a as the minimum shortening rate [*Thompson et al.*, 2002].

4. Shortening Along the Tuomuluoan Thrust Since ~0.35 Ma

[16] The SE-trending Tuomuluoan anticline lies immediately east of the Mayikake basin and is bounded by the Kezilesu River on the north (Figure 3a). The core of the anticline exposes highly deformed Paleogene massive gypsum, limestone, and mudstone. The northern margin of the anticline is defined by the Tuomuluoan Thrust (TT, the local name for this segment of the PFT) with an arcuate surface trace convex to the northeast (Figure 3a). To the east, the TT splays into two branches. The south branch displays a ~1-m-thick gouge zone and thrusts Paleogene strata over Quaternary conglomerates. The north branch, which slipped during the 1985 M7.4 Wuqia event (Figure 3a) [*Feng*, 1994], cuts the south limb of the Mingyaole anticline and produces a series of thrust scarps on the surface.

[17] The Mingyaole anticline, overridden by the Tuomuluoan anticline along the TT, is a geometrically simple detachment fold, which exposes Neogene strata in its core and Pleistocene conglomerates in each limb (Figure 3a) [*Scharer et al.*, 2006]. Since the initiation of fold growth at ~1.6 Ma, the Mingyaole anticline has accommodated a total shortening of ~1.5 km at a mean shortening rate of ~0.9 mm/a [*Chen et al.*, 2005]. On the Mingyaole's south limb, Plio-Pleistocene conglomerate is overthrusted along the TT by Paleogene gypsum of the Tuomuluoan anticline (Figure 3b). The fault dips ~16° to south, subparallel with underlying and overlying bedding. Interpretation of our new field mapping indicates ~2.1 km of overlap of Pleistocene conglomerates by overthrust Paleogene strata (Figure 3a). Given the 16° dip of the Tuomuluoan thrust, the minimum cumulative dip slip is ~2.2 km since deposition of the youngest footwall conglomerates.

[18] We constrained the age of the conglomerates with a new magnetostratigraphy spanning a 2.1-km-thick section underlying the TT along the southwestern margin of the Mingyaole anticline (Figure 3a). Detailed descriptions of sampling, measurement results, and analytical tests are shown in auxiliary material. The resulting magnetic polarity

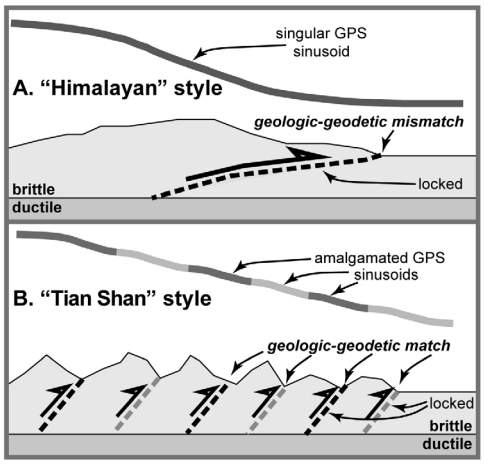

Figure 4. Conceptual model for contractional orogens of the (a) "Himalayan" and (b) "Tian Shan" type with a focus on the present or absence of a geologic-geodetic mismatch along major thrust faults.

sequence comprises seven magnetozones defined by two or more sites of similar polarity (Figure 3c). Our correlation to the geomagnetic polarity time scale of *Lourens et al.* [2004] is guided in part by the previously determined magnetostratigraphic age of strata in the same south limb of the Mingyaole anticline (Figure 3a) [*Chen et al.*, 2005] that we consider as coeval with the lower part of our new section. Our resulting correlation suggests that the new section extends from ~2.15 Ma to sometime in the Brunhes chron (0.78–0 Ma). Similar lithologic characteristics between the lower 1600 m and upper 500 m (Figure 3c) and a nearly uniform compacted sediment-accumulation rate in the lower part (Figure 3d) make it reasonable to extrapolate the accumulation rate of ~1150 m/Ma from the lower 1600 m to the top of the exposed section. This extrapolation predicts a maximum age of ~0.35 Ma for the tilting and overthrusting conglomerates (Figure 3d). Given this maximum age and the minimum dip slip of ~2.2 km since then, we estimate dip-slip rate along the TT of ≥6.4 mm/a. Because the TT is interpreted to dip more gently at greater depths (Figure 1d), the shortening rate can be considered roughly equal to the dip-slip rate of ≥6.4 mm/a [*Thompson et al.*, 2002].

5. Discussion and Conclusion

[19] Recent deformation along the northern margin of Chinese Pamir is concentrated on the PFT, a thrust activated in the latest foreland-ward propagation sequence of the Pamir. In the Mayikake basin, shortening is accommodated by the Biertuokuoyi Frontal Thrust and the Mayikake Thrust, with a total rate of ~6.0 mm/a (~2.9 mm/a and ~3.0 mm/a, respectively) since ~18.4 ka. To the east, shortening rate of the Tuomuluoan Thrust is ≥6.4 mm/a over the past ~0.35 Ma. These geologic rates of ~6–7 mm/a at two time scales are comparable to the geodetic rate of ~6–9 mm/a across this same zone. Any remaining discrepancy in rates could be accounted for by the broader zone spanned by the GPS sites (Figures 1a and 1c): a zone including several undated, but active thrust faults neighboring the STST [*Scharer et al.*, 2006]. We, therefore, conclude that average shortening rates have been equivalent across the PFT system since at least ~0.35 Ma. Slip cessation along the MPT and its southeast extension: the Kashgar-Yecheng Transfer System (Figure 1a) which is the Pamir-Tarim boundary fault [*Cowgill*, 2010; *Sobel et al.*, 2011], and the subsequent activation of the PFT due to northward migration of the deformation front may result from collisional interference between the Pamir and Tarim since late Miocene-Pliocene [*Sobel et al.*, 2011].

[20] In the Kyrgyz Alai Valley, ~150 km west of the Mayikake basin (Figure 1a), the PFT has become inactive and deformation has stepped hindwards to the MPT, which has a Holocene shortening rate of ~5.3 mm/a [*Arrowsmith and Strecker*, 1999]: similar to the rates determined in this study. Therefore, recent shortening rates along northern margin of the Pamir appear roughly uniform in space, in spite of accommodation by different deformation styles and an evolving spatial distribution. These rates are, however, strikingly higher than the average shortening rate of ~0.8 mm/a across this orogenic swath over the past 25 Ma [*Coutand et al.*, 2002]. This mismatch reflects an unsteady Late Cenozoic shortening history, such that recent rates are significantly faster than Miocene and older rates: a conclusion analogous to that observed in the Tian Shan [*Bullen et al.*, 2001; *Heermance et al.*, 2008]. Our results suggest that, in the Pamir and Tian Shan, geodetic rates can be used as proxies for geologic shortening rates at time scales up to perhaps one million years, but these rates commonly include much greater variability at orogenic time scales.

[21] At interseismic time scales, the equivalency of geologic and geodetic rates depends on the deformation pattern resulting from elastic strain accumulation (Figure 4). Fault geometry is a key controlling factor. The large mismatch in the Himalaya is interpreted to result from the presence of a low-angle locked megathrust (Figure 4a) [*Cattin and Avouac*, 2000; *Avouac*, 2003]: the Main Frontal Thrust (MFT) resembles a thin-skinned thrust, such that elastic strain accumulated across the Greater Himalaya is episodically released in large earthquakes that translate slip to the MFT. The mismatch of the Chelungpu Fault in Taiwan may also be interpreted as due to the presence of extensive low-angle faults [*Dominguez et al.*, 2003]. In contrast, the Tian Shan, where geodetic and geologic rates appear to match in Late-Quaternary [*Thompson et al.*, 2002], is a thick-skinned orogen comprising faults that are relatively closed spaced and steeply dipping through the brittle crust (Figure 4b). We speculate that deformation in the northern Pamir scales with the thickness of the seismogenic brittle crust, as it does in the Tian Shan. In the Himalaya, however, the seismogenic portion of the low-angle Main Himalaya Thrust (which connects to the MFT) extends beneath the orogen for up to 200 km. Across this region, this fault evolves from a relatively weak, creeping fault in the ductile crust to a locked fault in the brittle crust, such that slip and elastic strain are differentially accommodated along the fault [*Cattin and Avouac*, 2000; *Avouac*, 2003]. Overall, comparison of different contractional orogens suggests that fault geometry, mechanics, and spacing determine whether an equivalence between geologic and geodetic rates is easily recognized. We conjecture that these rates are more likely to be equivalent where faults dip relatively steeply, fault splays are numerous, fault spacing is close, and fault-related deformation scales with the thickness of seismogenic brittle crust (Figure 4).

[22] **Acknowledgments.** This study was completed while Li was hosted at UC Santa Barbara and was supported by International Science and Technology Cooperation Program of China (2008DFA20860), a grant from State Key Lab. of Earthquake Dynamics of China (LED2010A04), and the US NSF (EAR 1050070). Li and Thompson acknowledge support from a CSC and NSF graduate research fellowship, respectively. We thank J. Kirschvink and T. Raub for use of the Caltech paleomagnetics lab, C. Jones for use of his software in our magnetostratigraphic analysis, and Chen Ji (UCSB) for the half-space modeling. We also thank Wang C., Yang H. and Yang X. for their help in processing OSL samples. Critical and thorough reviews of the manuscript by W. Hammond and an anonymous reviewer significantly improved the current version.

[23] The Editor thanks William Hammond and Michael Hamburger for assisting in the evaluation of this paper.

References

Abdrakhmatov, K. Y., et al. (1996), Relatively recent construction of the Tien Shan inferred from GPS measurements of present-day crustal deformation rates, *Nature*, *384*, 450–453, doi:10.1038/384450a0.

Arrowsmith, J. R., and M. R. Strecker (1999), Seismotectonic range-front segmentation and mountain-belt growth in the Pamir-Alai region, Kyrgyzstan (India-Eurasia collision zone), *Geol. Soc. Am. Bull.*, *111*, 1665–1683, doi:10.1130/0016-7606(1999)111<1665:SRFSAM>2.3.CO;2.

Avouac, J. P. (2003), Mountain building, erosion, and the seismic cycle in the Nepal Himalaya, *Adv. Geophys.*, *46*, 1–80, doi:10.1016/S0065-2687(03)46001-9.

Bullen, M. E., D. W. Burbank, J. I. Garver, and K. Y. Abdrakhmatov (2001), Late Cenozoic tectonic evolution of the northwestern Tien Shan: New age estimates for the initiation of mountain building, *Geol. Soc. Am. Bull.*, *113*, 1544–1559, doi:10.1130/0016-7606(2001)113<1544:LCTEOT>2.0.CO;2.

Burtman, V. S., and P. Molnar (1993), *Geological and Geophysical Evidence for Deep Subduction of Continental Crust Beneath the Pamir*, *Spec. Pap. Geol. Soc. Am.*, *281*, 76 pp.

Cattin, R., and J. P. Avouac (2000), Modeling mountain building and the seismic cycle in the Himalaya of Nepal, *J. Geophys. Res.*, *105*, 13,389–13,407, doi:10.1029/2000JB900032.

Chen, J., K. M. Scharer, D. W. Burbank, R. Heermance, and C. S. Wang (2005), Quaternary detachment folding of the Mingyaole anticline, southwestern Tianshan [in Chinese], *Seismol. Geol.*, *27*, 530–547.

Chen, H. L., F. F. Zhang, X. G. Cheng, L. Liao, J. C. Luo, J. Shi, B. Q. Wang, C. F. Yang, and L. F. Chen (2010), The deformation features and basin-range coupling structure in the northeastern Pamir tectonic belt [in Chinese], *Chin. J. Geol.*, *45*, 102–112.

Coutand, I., M. R. Strecker, J. R. Arrowsmith, G. Hilley, R. C. Thiede, A. Korjenkov, and M. Omuraliev (2002), Late Cenozoic tectonic development of the intramontane Alai Valley, (Pamir-Tien Shan region, central Asia): An example of intracontinental deformation due to the Indo-Eurasia collision, *Tectonics*, *21*(6), 1053, doi:10.1029/2002TC001358.

Cowgill, E. (2010), Cenozoic right-slip faulting along the eastern margin of the Pamir salient, northwestern China, *Geol. Soc. Am. Bull.*, *122*, 145–161, doi:10.1130/B26520.1.

Dominguez, S., J.-P. Avouac, and R. Michel (2003), Horizontal coseismic deformation of the 1999 Chi-Chi earthquake measured from SPOT satellite images: Implications for the seismic cycle along the western foothills of central Taiwan, *J. Geophys. Res.*, *108*(B2), 2083, doi:10.1029/2001JB000951.

Feng, X. Y. (1994), Surface rupture associated with the 1985 Wuqia earthquake, in *Xinjiang: Research on Active Fault*, pp. 45–55, Seismological Press, Beijing.

Heermance, R. V., J. Chen, D. W. Burbank, and J. Miao (2008), Temporal constraints and pulsed Late Cenozoic deformation during the structural disruption of the active Kashi foreland, northwest China, *Tectonics*, *27*, TC6012, doi:10.1029/2007TC002226.

Lavé, J., and J. P. Avouac (2000), Active folding of fluvial terraces across the SiwaliksE Hills, Himalayas of central Nepal, *J. Geophys. Res.*, *105*, 5735–5770, doi:10.1029/1999JB900292.

Liu, J. F., J. Chen, J. H. Yin, Y. C. Lu, A. Murray, L. C. Chen, J. Thompson, and H. L. Yang (2010), OSL and AMS ^{14}C dating of Penultimate earthquake at the Leigu trench along the Beichun fault, Longmen Shan, in the northeast margin of the Tibetan Plateau, *Bull. Seismol. Soc. Am.*, *100*, 2681–2688, doi:10.1785/0120090297.

Lourens, L. J., F. J. Hilgen, J. Laskar, N. J. Shackelton, and D. Wilson (2004), The Neogene period, in *Geological Time Scale*, edited by F. M. Gradstein, J. G. Ogg, and A. Smith, pp. 409–440, Cambridge Univ. Press, Cambridge, U. K.

Lu, Y. C., X. L. Wang, and A. G. Wintle (2007), A new OSL chronology for dust accumulation in the last 130,000 yr for the Chinese Loess Plateau, *Quat. Res.*, *67*, 152–160, doi:10.1016/j.yqres.2006.08.003.

Petit, J. R., et al. (1999), Climate and atmosphere history of the past 420,000 years from the Vostok ice core, Antarctica, *Nature*, *399*, 429–436, doi:10.1038/20859.

Scharer, K. M., D. W. Burbank, J. Chen, and R. J. Weldon (2006), Kinematic models of fluvial terraces over active detachment folds: Constraints on the growth mechanism of the Kashi-Atushi fold system, Chinese Tian Shan, *Geol. Soc. Am. Bull.*, *118*, 1006–1021, doi:10.1130/B25835.1.

Segall, P. (2002), Integrating geologic and geodetic estimates of slip rate on the San Andreas Fault System, *Int. Geol. Rev.*, *44*, 62–82, doi:10.2747/0020-6814.44.1.62.

Sobel, E. R., and T. A. Dumitru (1997), Thrusting and exhumation around the margins of the western Tarim basin during the India-Asia collision, *J. Geophys. Res.*, *102*, 5043–5063, doi:10.1029/96JB03267.

Sobel, E. R., J. Chen, and R. V. Heermance (2006), Late Oligocene-early Miocene initiation of shortening in the southwestern Chinese Tian Shan: Implications for Neogene shortening rate variations, *Earth Planet. Sci. Lett.*, *247*, 70–81, doi:10.1016/j.epsl.2006.03.048.

Sobel, E. R., L. Schoenbohm, J. Chen, R. Thiede, D. Stickli, M. Sudo, and M. Strecker (2011), Late Miocene-Pliocene deceleration of dextral slip between Pamir and Tarim: Implications for Pamir orogenesis, *Earth Planet. Sci. Lett.*, *304*, 369–378, doi:10.1016/j.epsl.2011.02.012.

Thompson, S. C., R. J. Weldon, C. M. Rubin, K. Abdrakhmatov, P. Molnar, and G. W. Berger (2002), Late Quaternary slip rates across the central Tien Shan, Kyrgyzstan, central Asia, *J. Geophys. Res.*, *107*(B9), 2203, doi:10.1029/2001JB000596.

Yang, S. M., J. Li, and Q. Wang (2008), The deformation pattern and fault rate in the Tianshan Mountains inferred from GPS observations, *Sci. China, Ser. D*, *51*(8), 1064–1080, doi:10.1007/s11430-008-0090-8.

Yin, A., S. Nie, P. Craig, T. M. Harrison, F. J. Ryerson, X. Qian, and G. Yang (1998), Late Cenozoic tectonic evolution of the southern Chinese Tian Shan, *Tectonics*, *17*(1), 1–17, doi:10.1029/97TC03140.

Zubovich, A. V., et al. (2010), GPS velocity field for the Tien Shan and surrounding regions, *Tectonics*, *29*, TC6014, doi:10.1029/2010TC002772.